Study on Seepage Characteristics of High Core Rockfill Dam under Aging and Dissolution of Impervious Body

Kai Zhang[1,*], Baofeng Xie[2], Guanzhou Li[2], Dongyang Qin[3]

[1]Nanjing Hydraulic Research Institute, Nanjing, 210029, China
[2]Yellow River Water Resources and Hydropower Development Group Co., Ltd., Zhengzhou, 450047, China
[3]College of Water Conservancy and Hydropower Engineering, Hohai University, Nanjing, 210024, China
*Corresponding author. E-mail: kzhang@nhri.cn

Abstract. Impervious body is the key line of defense to ensure the long-term service safety of earth-rock dams, but the seepage dissolution easily leads to the deterioration of the performance of impervious body, which in turn leads to the failure of seepage control system and the seepage damage of dam foundation. This paper takes a certain hydraulic project as the research object and comprehensively considers multi-source information, including topography, stratigraphic lithology, faults, hydrogeology, in-situ tests, locations of hydraulic structures, and the grout curtain, to establish a high-precision three-dimensional numerical seepage model that encompasses the dam body, dam foundation, abutment mountains, faults, drainage tunnels, seepage control facilities, and the sediment layer. Based on monitoring data from piezometers and seepage discharge measurements, a structural-plane-controlled back-analysis method was adopted to identify and validate the model parameters, thereby enhancing the accuracy and reliability of the model. Using the calibrated numerical model, the evolution of the seepage field was simulated under various operating conditions, including the design normal storage level, variations in sediment layer thickness, and partial failure of the grout curtain. The distribution of the seepage field, changes in seepage discharge, hydraulic gradient characteristics, and the performance of the seepage control system were thoroughly analyzed. The research findings can provide a scientific basis for the safe operation and full benefit realization of the project.

Keywords: High core rockfill dam; dissolution aging; impervious body; seepage analysis; numerical model

1 Introduction

Embankment dams have found extensive application in large-scale water conservancy projects, attributed to their merits such as abundant sources of construction materials, favorable adaptability to diverse topographical and geological settings, and superior earthquake resistance[Wang.2013]. As an important hydraulic structure widely used in hydraulic engineering, its seepage characteristics are directly related to the structural

© The Author(s) 2026
H. Wu et al. (eds.), *Proceedings of the 2026 3rd International Conference on Civil Engineering Structures and Concrete Materials (CESCM 2026)*, Advances in Engineering Research 312,
https://doi.org/10.2991/978-94-6239-865-8_13

stability and long-term service safety of dam body. The seepage control system of embankment dams is primarily composed of the impervious structures within the dam body and those within the dam foundation. The dam-body impervious structures include clay cores, clay inclined cores, asphalt concrete cores, concrete face slabs, and other forms. However, in the long-term service process, due to the influence of water erosion, chemical dissolution and particle migration, the internal structure of the material may change, leading to the deterioration of permeability, which in turn affects the seepage safety of the dam.

In the study of seepage characteristics of earth-rock dams, Ahmed et al. [Janabi.2024] evaluated the ability and accuracy of the numerical model based on SEEP/W software in predicting the saturation line and permeability of homogeneous earth-rock dams. Dai et al [Dai et al.2023] used EFGM to solve the problem of saturated-unsaturated seepage field, and obtained the steady-state zero pressure surface and overflow point. Although it lays a foundation for accurate characterization and numerical simulation of seepage field, it mainly focuses on the instantaneous or short-term hydraulic behavior of embankment dams, and does not fully consider the performance evolution of seepage body during long-term service. With the increase of dam service life, the structural durability problems caused by long-term seepage gradually become prominent, and the research focus gradually shifts from simple field analysis to exploration of seepage dissolution coupling mechanism. Zhao et al. [Zhao.2024] studied the seepage and dissolution characteristics of a reservoir in Shanxi by constructing a stochastic model of seepage and dissolution coupling. Zhang et al. [Zhang.2025] studied the evolution characteristics of seepage dissolution and the evolution law of seepage resistance of concrete cutoff wall; Zaher et al. [Yaseen.2026] summarized the progress of seepage analysis with AI in recent years, which can be used as a guide to predict the potential of AI-driven seepage. Zhou et al. [Zhou.2025] established a coupling model of dissolution-seepage-stress in saturated-unsaturated porous media to simulate the dissolution process of plastic concrete cutoff wall (PCCW). Based on saturated-unsaturated seepage theory and calcium dissolution-migration theory, Zhang et al. [Zhang.2025] established a seepage-dissolution coupling model, and put forward a numerical method to quantify the influence of calcium dissolution on the service performance of concrete cutoff wall. Huo et al [Huo.2019] established a multi-field coupling model, and obtained the attenuation trend of dam foundation curtain performance under groundwater erosion.

However, existing studies predominantly focus on the independent leaching degradation of single specific anti-seepage structures (e.g., concrete cut-off walls or foundation grout curtains). They have neither developed a refined 3D numerical simulation that incorporates the combined anti-seepage system of the dam core and foundation into a unified analytical framework, nor considered the multi-factor coupled boundary conditions—including significant water-level fluctuations induced by water and sediment regulation, reservoir sedimentation, and localized structural failures—to conduct lateral quantitative comparisons of the relative risks of permeability degradation across different seepage-control components. Consequently, it remains difficult to quantitatively assess the threat that the progressive deterioration of the seepage-control system poses to the overall seepage safety of the earth-rock dam site during long-term operation.

To remedy the above shortcomings, this study, based on an actual hydraulic engineering project, systematically examines the seepage response characteristics of different seepage-control components within the dam body and foundation under diverse aging and leaching scenarios. A refined three-dimensional numerical seepage model of the study area was established using the FORTRAN language. Specific methods were adopted for handling drainage holes, determining cross-section flow rates, locating the free surface, and identifying seepage exit points. Furthermore, the model parameters were identified and validated by means of a structural plane-controlled inversion method, thereby enhancing the accuracy and reliability of the model. The seepage variation law in the study area is simulated and predicted under the conditions of normal design water level, thickness change of siltation layer and partial failure of seepage prevention curtain, and the seepage field, seepage quantity, hydraulic gradient change law and seepage prevention and drainage effect in the study area are deeply analyzed, and the effect of seepage prevention system of the water control project is evaluated. The research results can provide theoretical basis for seepage safety evaluation of high-core earth-rock dam in long-term operation.

2 Model and Method

2.1 Mathematical Model and Solution

The hinge region is heterogeneous and anisotropic. The mathematical model of unsteady motion of three-dimensional seepage can be expressed by equation (1).

$$\begin{cases} \mu_s \dfrac{\partial H}{\partial t} = \dfrac{\partial}{\partial x}\left(K_x \dfrac{\partial H}{\partial x} \right) + \dfrac{\partial}{\partial y}\left(K_y \dfrac{\partial H}{\partial y} \right) + \dfrac{\partial}{\partial z}\left(K_z \dfrac{\partial H}{\partial z} \right) + \varepsilon, \quad x, y, z \in \Omega, \quad t \geq 0, \\ H\left(x, y, z, t\right)\big|_{t=0} = H_0, \quad x, y, z \in \Omega, \quad t \geq 0, \\ K_n \dfrac{\partial H}{\partial \vec{n}}\bigg|_{\Gamma_1} = q\left(x, y, z, t\right), \quad x, y, z \in \Gamma_1, \quad t \geq 0 \end{cases} \tag{1}$$

where Ω—Seepage area; H—water level elevation of aquifer; Kx, Ky and Kz—permeability coefficients in x, y and z directions respectively; μs-water storage rate; ε - Source and sink terms of aquifer; H_0 —initial water level distribution of aquifer; Γ_1— The second boundary of seepage area, including the water-resisting boundary at the bottom of confined aquifer and the lateral flow or water-resisting boundary of seepage area; n— the normal direction of the boundary surface; K_n refers to the permeability coefficient in the normal direction of the boundary surface; $Q(x, y, z, t)$ —is defined as the flow per unit area of the second boundary, with positive inflow, negative outflow and zero water-resisting boundary.

By finite element discretization of equation (1), algebraic equation (2) of the whole seepage region is obtained.

$$[G]\{H\}+[P]\{\frac{dH}{dt}\}=\{F\} \tag{2}$$

where: *[G]*—global permeability matrix (conduction matrix);*[P]*—storage matrix;*{H}*—unknown nodal head array;*{F}*—known right hand term.

For $\frac{dH}{dt}$, take the difference instead:

$$\frac{dH}{dt}=\frac{H_{(t+\Delta t)}-H_{(t)}}{\Delta t} \tag{3}$$

Using "implicit difference scheme", there are

$$[G]\{H_{t+\Delta t}\}+[P]\{\frac{H_{(t+\Delta t)}-H_t}{\Delta t}\}=\{F\} \tag{4}$$

Rearranging gives Equation (5).

$$\{[G]+\frac{1}{\Delta t}[P]\}[H_{t+\Delta t}]=\frac{1}{\Delta t}[P]\{H_t\}+\{F\} \tag{5}$$

2.2 Drainage Hole Treatment Method

Drainage tunnels are set in the left and right bank of the dam, with drainage holes with a diameter of 110mm and a hole spacing of 3.0m, and combined filters are placed in the drainage holes located in the fault zone and the clay strata on the right bank to prevent seepage damage. For these drainage holes, the rod element method is adopted, and the specific method is illustrated by taking a typical element as an example: consider the hexahedral element (Figure 1) and assume that the node 1485 of the element is the section where the drainage hole is located.

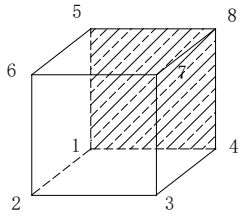


Fig. 1. Typical Unit Diagram for Drainage Hole Treatment

The permeability matrix (6) of the member element is distributed to the four nodes 1, 4, 8 and 5 of the typical element matrix. Specifically, ps is added or subtracted from the diagonal elements a_{11}, a_{44}, a_{88} and a_{55} of the permeability matrix (8×8) of the typical element.

$$K_{\omega} = p_s \begin{bmatrix} 1 & -1 \\ -1 & 1 \end{bmatrix} \tag{6}$$

$$p_s = \frac{K\Delta F}{\Delta l_s} \tag{7}$$

$$\Delta l_s = \frac{b}{2\pi} \ln \frac{b}{2\pi\gamma_{\omega}} \tag{8}$$

$$K = \sqrt[3]{K_1 K_2 K_3} \tag{9}$$

where b—well (hole) spacing, γ_{ω}—well (hole) radius, K—permeability coefficient, K_1, K_2, K_3—three main permeability coefficients of rock mass respectively, ΔF—unit section area where hole is located.

2.3 Determination of Cross-Section Flow

Since the partial derivatives of the hydraulic head with respect to the coordinates at the element nodes cannot be obtained directly when using the finite element method to solve the seepage field, the mid-section method is adopted for calculating the flow rate across a cross-section.

Taking the 8-node flow surface element as an example, the calculation formula of seepage flow through a certain section S is as follows

$$q = -\int_S K_n \frac{\partial H}{\partial n} ds = -K_n S \frac{\partial H}{\partial n} \tag{10}$$

where S—water flow section; n—unit vector in the normal direction of the water flow section. For any eight-node hexahedron isoparametric element, choose the middle section abcd as the over-current section S, and project S on the planes of yoz, zox and xoy, which are denoted as Sx, Sy and Sz respectively, then the seepage through the middle section of the element is

$$q = -K\left(\frac{\partial H}{\partial x} S_x + \frac{\partial H}{\partial y} S_y + k_z \frac{\partial H}{\partial z} S_z\right) \tag{11}$$

where $\frac{\partial H}{\partial x}$, $\frac{\partial H}{\partial y}$ and $\frac{\partial H}{\partial z}$ are calculated by the following formula.

$$\left[\frac{\partial H}{\partial x}, \frac{\partial H}{\partial y}, \frac{\partial H}{\partial z}\right]^T = \left[\frac{\partial N_i}{\partial x}, \frac{\partial N_i}{\partial y}, \frac{\partial N_i}{\partial z}\right]^T \cdot \left[H_i\right] \tag{12}$$

2.4 Determination of Free Surface and Seepage Point

The surface that satisfies the condition h=z is defined as the free surface. In practical problems, its initial position is unknown, and the free surface can be obtained iteratively by combining the flow of alternative nodes in the analysis process. At this point, the boundary of the computational domain completely above the free surface can be regarded as the impervious surface in the first iteration. The head distribution can be obtained by solving equation (5) for the selected calculation domain. It can be considered that the nodes above the free surface all have a negative head, and the head of these nodes is smaller than the corresponding elevation. This area is the first approximation of the area actually located above the infiltration area. However, there is still an error in such an analysis, because the cells in this region have an influence on equation (5). For the element *e* in which the head of all nodes is negative, it is equal to

$$[C^{e'}]\{h^{e'}\} = \{\overline{Q}^{e'}\} \tag{13}$$

The flow correction vector $\{\overline{Q}_n\}$ can be obtained by summing the $\{\overline{Q}^{e'}\}$ of all elements with negative node head.

$$\{\overline{Q}_n\} = \sum_{e'} \{\overline{Q}^{e'}\} = \sum_{e'} [C^{e'}]\{h^{e'}\} \tag{14}$$

The solution of equation (13) gives a new potential distribution, and the position of the free surface is improved compared with that of the first iteration. A new flow correction vector can be obtained from the newly obtained hydraulic head, and then Equation (13) can be solved. If this is repeated, the change of hydraulic head is usually very small only after several iterations, and the position of the free surface can be obtained. The position of seepage point is related to the form of drainage. The seepage point is both a point on the free surface of seepage and a point on the seepage section. Since the seepage point is a point on the seepage free surface, it can be calculated iteratively with the nodes on the seepage free surface.

2.5 Discontinuities-Control Inverse Analytic Method

According to the observed and calculated values of hydraulic head at known coordinate positions in the calculation area, as well as the errors between the observed and calculated values of leakage of dam foundation and left and right bank drainage tunnels, the objective function is established by least square method:

$$E(K_j^i) = \sum_{k=1}^{M} \omega_k \sqrt{(H_k^c - H_k^o)^2} + \sum_{l=1}^{N} \omega_l \sqrt{(Q_l^c - Q_l^0)^2} \tag{15}$$

Where: K_j^i— is the parameter to be solved, superscript *i* represents the *i-th* sub-region divided according to the water permeability of rock mass, *i* = *I*, *II*, …, *NNO*, *NNO*

is the total number of sub-regions, subscript J represents the *j-th* parameter in the *i-th* sub-region, and $j = 1,2, \ldots, NK$, NK is the total number of parameters in a certain region;

ω_K and ω_L are the weight functions of the *k-th* hydraulic head observation point and the *l-th* flow observation value respectively, and there are $\sum_{k=i}^{M} \omega_k = 1.0$; $\sum_{l=1}^{N} \omega_l = 1.0$. *m* and *n* are the total number of observation points (holes) in the area respectively; H_k^c、H_k^0— the calculated value and the observed value of the hydraulic head at the *k-th* observation point in the region, respectively; Q_l^c, Q_l^c— calculated value and measured value of the *l-th* flow observation point in the area, respectively. Obviously, from the above constraints, a set of parameters can be found to make the objective function *E* tend to 0.

3 General Situation of Study Area

A water conservancy project is a large (1) type comprehensive utilization water conservancy project. The normal storage level of this hydraulic project is 275.00 m, and the downstream water level is 138.5 m. A concrete cutoff wall with a hole depth of 82m and a thickness of 1.2m and bedrock curtain grouting are used to prevent seepage at the dam foundation. The concrete cutoff wall is inserted upward into the inclined core wall for 12m and downward into the bedrock for 1m~2m to form the main vertical antiseepage system of the main dam. The silt sedimentation in front of the dam and the loam inclined wall of the flood cofferdam are used to form a horizontal auxiliary antiseepage system. Two vertical seepage control treatments are adopted for the deep gravel overburden of the main dam foundation. Under the inclined wall of the upstream cofferdam, the seepage control measures of plastic concrete cutoff wall and high-pressure jet grouting curtain are adopted. The main dam is filled by 17 kinds of dam materials, of which the intercepting dam and the cofferdam are part. The typical section is shown in Fig 2.

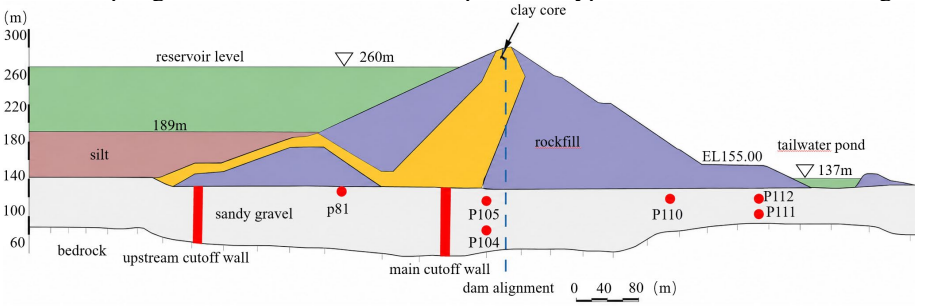


Fig. 2. Typical profile of main dam

The bedrock exposed in the dam site area is a set of red clastic rock series, and its main lithology is sandstone, claystone and interbedded sandstone and claystone. There are mainly two groups of fault structures, and the structural cracks are mainly steep dip.

The density of cracks in hard sandstone is high, and the development of cracks in soft rocks such as clay rock and argillaceous siltstone is poor, which makes the water permeability of hard rock layer obviously stronger than that of soft rock. Given that sandstone is more fissured than claystone and shale, a layered distribution of rock types results in a corresponding layered permeability. Table 1 lists the layered permeability values of the rock strata obtained from the original site investigation data. Due to the effects of weathering and unloading, the permeability of the rock strata decreases significantly from the surface downward. The statistics of the permeability variation with depth for the left bank rock strata, obtained from borehole packer (water pressure) tests, are presented in Table 2. From the boreholes located near the F_1 fault, it can be seen that the rock mass above 80m below the rock surface has strong to extremely strong water permeability.

Table 1. Stratified distribution of permeability

Rock group code	Permeability category	Sandstone content	Mudstone content	Hydraulic conductivity parallel to bedding	Hydraulic conductivity perpendicular to bedding	Anisotropy ratio
T_1^5	Sandstone-mudstone type	71%	29%	0.64	0.0061	104.1
T_1^4	Sandstone type	95%	5%	0.62	1.04	0.6
T_1^{3-2}	Mudstone type	43%	57%	0.0009	0.0015	0.5
T_1^{3-1}	Sandstone type	90%	10%	0.42	0.71	0.6
T_1^{2-1}	Sandstone-mudstone type	52%	49%	0.05	0.0049	10.2

Table 2. Statistics of water permeability variation with depth

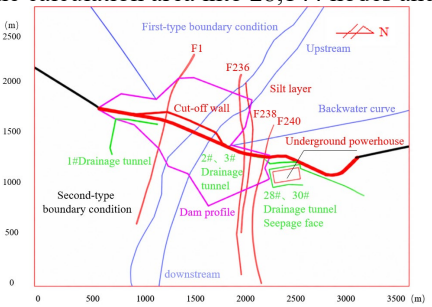
Permeability layer	Bottom elevation(m)	Thickness(m)	Lugeon value(Lu)
Highly permeable layer	250.00~275.00	8~20	46
Moderately permeable layer	221.69~255.00	6~54	7
Weakly permeable layer	243.00~275.00	7~110	3

4 Model Parameter Identification

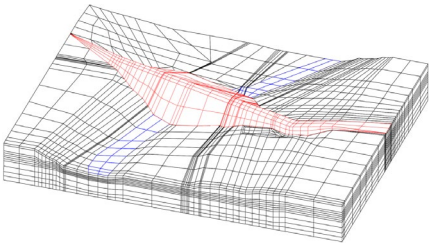
4.1 Model Scope and Boundary Conditions

Based on the geological conditions of the project area and the layout characteristics of the hydraulic structures, the computational domain was determined. The domain extends 1200.0 m upstream and 1200.0 m downstream from the dam body, and 500.0 m outward from both the left and right abutments along the grout curtain. The resulting model domain measures 3600.0 m (in the north–south direction) × 2700.0 m (in the east–west direction) (Figure 3(a)). The model primarily incorporates the dam body, dam foundation, the seepage control systems on both abutments, the upstream concrete cutoff wall, the sediment layer, drainage tunnels Nos. 1~4, 28, and 30, Faults F_1 and F_{236}~F_{240}, as well as the underground powerhouse, among others. The upstream reservoir backwater line is the first boundary, the downstream river is the first boundary,

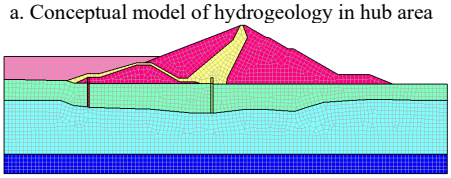
and the mountains on both sides are the second boundary. The top of the model receives rainfall infiltration recharge, and the bottom is the water-proof boundary. Take the coordinate system with the X axis pointing due north, the Y axis pointing due west and the Z axis pointing vertically upwards as the calculation coordinate system, and divide the calculation area into 28,144 nodes and 26,313 units, as shown in Figure 3(b~d).



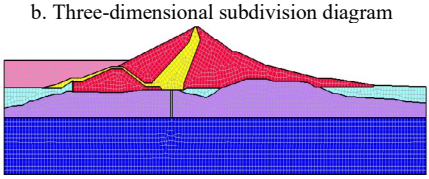
a. Conceptual model of hydrogeology in hub area



b. Three-dimensional subdivision diagram



c. B-B section



d. C-C section

Fig. 3. computational domain

4.2 Initial Material Parameters

Table 3. List of initial values of permeability coefficient of each material

Location	Material No.	Material Name	Permeability Coefficient (cm/s)
Dam body	1	Clay core	$(1.0\sim9.9)\times10^{-7}$
	2	Filter material	$(1.0\sim5.0)\times10^{-6}$
	3	Rockfill	1.0×10^{-1}
	4	Dam cutoff wall	1.0×10^{-8}
	5	Clay blanket	1.0×10^{-5}
	6	Cofferdam cutoff wall	1.0×10^{-6}
Dam foundation	7	Pre-dam siltation layer	$(1.0\sim9.9)\times10^{-5}$
	8	Riverbed overburden	$(1.0\sim5.0)\times10^{-2}$
	9	Foundation seepage control	2.0×10^{-5}
Fault	10	F_1	1.0×10^{-5}
	11	F_{236}	$5.0\times10^{-3}\sim5.0\times10^{-4}$
	12	F_{238}	$5.0\times10^{-3}\sim5.0\times10^{-4}$
	13	F_{240}	$5.0\times10^{-3}\sim5.0\times10^{-4}$
Abutment rock mass	14	P_2^1 Shale	2.0×10^{-4}
	15	P_2^2 Fine sandstone	8.0×10^{-5}
	16	P_2^3 Interbedded layers	5.0×10^{-5}
	17	P_2^4 Clay	1.0×10^{-6}
	18	Rock group T	1.0×10^{-6}

This model mainly considers the materials such as stratum lithology, underground powerhouse, dam body, dam foundation, mountains on both banks, faults, drainage tunnels, anti-seepage facilities, siltation layer, etc. On the basis of geological drilling data and construction quality inspection records of dam embankment placement, the preliminary bounds of the model parameters were established. (Table 3).

4.3 Model Parameter Identification Results

Table 4. Comparison of measured and calculated water levels of each osmotic pressure gauge at B-B section

Osmometer number	Monitoring time: January 30, 2021		June 27, 2021		October 29, 2021	
	measured value (m)	calculated value (m)	measured value (m)	calculated value (m)	measured value (m)	calculated value (m)
water level	267.00	267.00	241.00	241.00	269.50	269.50
P104	139.67	141.15	139.38	140.52	139.71	141.21
P105	141.94	139.97	141.57	139.57	142.05	140.01
P111	138.00	138.50	138.00	138.40	138.11	138.51
P116	271.29	223.66	254.39	206.39	271.49	225.32
P117	264.98	195.33	243.90	183.78	265.33	196.44
P124	249.18	267.00	246.66	241.00	239.74	269.50
P125	238.88	236.23	236.89	234.55	239.31	236.46
P130	271.13	267.00	244.73	241.0	273.48	269.50
P131	271.00	267.00	250.00	anhydrous	273.06	269.50
P133	271.42	267.00	250.00	anhydrous	273.71	269.50

Table 5. Comparison of measured and calculated water levels of various osmotic pressure gauges at C-C section

Osmometer number	Monitoring time: January 30, 2021		June 27, 2021		October 29, 2021	
	measured value (m)	calculated value (m)	measured value (m)	calculated value (m)	measured value (m)	calculated value (m)
water level	267.00	267.00	241.00	241.00	269.50	269.50
P140	264.94	267.00	238.83	241.00	267.21	269.50
P144	196.97	189.01	182.90	177.68	198.38	190.10
P145	192.25	194.04	179.68	181.76	194.39	195.22
P148	138.28	136.51	137.83	137.02	138.54	138.65
P150	140.17	136.05	139.75	136.38	139.94	136.12
P152	195.30	194.58	184.37	183.57	196.80	195.70
P161	227.46	226.12	219.81	218.24	227.99	226.48

On October 9, 2021, the reservoir water level reached a record high of 273.50m, so the observed values of osmometers and seepage flow in 2021 were selected to fit the model parameters, including 10 osmometers in section B-B, 7 osmometers in section C-C, and

3 osmometers in the right bank. The seepage quantity is considered in the left bank drainage tunnel, the right bank No.1 tunnel and the dam foundation. The observation time of osmometer and leakage is from January 1 to December 31, 2021. The leakage and measured water level behind the dam at these observation time points are calculated, and the calculated values and measured values are used for fitting. Three typical times in 2021, January 30, June 27 and October 29, are selected, and the calculated water levels and measured values are shown in Table 4 and Table 5.

It can be seen from the table that P104, P105, P111, P125, P130, P131 and P131 fit well with the measured values of osmometer, but P116, P117 and P124 fit poorly because the calculation cannot effectively simulate the situation that the pore water pressure is not dissipated. P116 and P117 are inside the core wall, because the permeability of the core wall is very small, the hydraulic head is obviously reduced, and the high pressure may be due to the rolling of the core wall during construction, and the pore water pressure has not completely dissipated. P124 is located in the transition material of clay core wall, which has great permeability, so the calculated water level is basically consistent with the reservoir water level. Except P144, the other osmometers of section C-C fit well.

Drainage tunnel on the left bank, No.1 tunnel on the right bank and dam foundation seepage are selected for flow fitting (Table 6). It can be seen from the table that the calculated results of leakage are basically consistent with the measured values. It shows that the parameter values retrieved through the osmometer and flow fitting are reasonable, and the identified model can be used for simulation and prediction of groundwater seepage field of the hub.

Table 6. Comparison of measured and measured leakage

Leakage monitoring location	Monitoring time			
	January 17, 2021		June 6, 2021	
	measured value (m)	Calculated value (m)	measured value (m)	Calculated value (m)
water level	264.92	264.92	260.130	260.13
left bank drainage tunnel	6130	6135.22	4644	4647.51
Hole 1 on the right bank	2371	2374.15	2575	2578.39
dam foundation seepage	7495	7491.67	8090	8092.14
total leakage	15996	16001.04	15309	15318.04

5 Calculation Result

The 3-D seepage field numerical model determined by inversion is used to simulate and predict the variation law of groundwater flow field, considering the influence of seepage prevention and drainage facilities, reservoir water level and faults on seepage field, hydraulic gradient, leakage amount and head reduction. In order to show the simulation results directly, three typical sections are selected in the calculation model: B-B section and C-C section are located in the dam body; LL section is located on the left bank and passes through the underground powerhouse. There are 14-16 characteristic points, numbered as points A~ P and points A'~ N', mainly located at cofferdam impervious

wall, dam foundation impervious wall, core wall, downstream escape source and upstream siltation layer.

The overburden layer of the dam foundation is relatively thick; therefore, a concrete cutoff wall was installed 80 m upstream of the dam axis, with a permeability coefficient of 1.0×10^{8} cm/s. This calculation also takes into account the possible corrosion aging of the impervious wall after many years of operation, and the variation law of leakage amount and water level when the permeability coefficient is increased by 5 times, 10 times and 100 times respectively[Wang.2017] (at this time, it is the same as the permeability coefficient of the impervious wall of the upstream cofferdam).

The core wall of the dam is mainly composed of clay, and its permeability coefficient is 1.0× 10-7 cm/s. This study considers the possibility of partial aging of clay core wall, that is, the variation law of hydraulic gradient and free surface when permeability coefficient increases 5 times, 10 times and 20 times respectively (it is the same as that of filter material of dam body).

The F1 fault is developed on the right bank. The fracture zone is wide, about 7~15m. Concrete was poured in the relevant parts during the construction, and its permeability coefficient is 1.0×10^{-5}cm/s. Considering the possibility and most adverse effects of dissolution and aging, the permeability coefficient is 2 orders of magnitude larger than before dissolution and aging, which is 3.0×10^{-3}cm/s.

The seepage control in front of underground powerhouse is mainly dam foundation and both banks, and the permeability coefficient is 2.0× 10-5 cm/s. Considering the dissolution and aging conditions, the leakage and water level change law when the permeability coefficient increases by 5 times, 10 times and 20 times respectively.

Before the flood season in 2022, the measured elevation of siltation layer in front of the main dam was 200.99m. In this study, the variation patterns of seepage discharge and hydraulic gradient are examined when the sediment layer thickness is increased by 5 m, 10 m, and 20 m, respectively.

6 Analysis and Discussion

6.1 Seepage Field and Seepage Stability Analysis

Overall, the groundwater level gradually decreases from the upstream side toward the downstream side after passing through the dam body, dam foundation, and abutment rock masses on both banks, with relatively pronounced foundation seepage and bypass seepage around the dam. The seepage control system, consisting of the upstream sediment layer, cofferdam cut-off wall, foundation cut-off wall, and core wall, contributes substantially to hydraulic head dissipation. Under the normal pool level of 275.00 m, the sediment layer dissipates approximately 70% of the hydraulic head in Section BB and approximately 40% in Section CC. The overall seepage control system can dissipate more than 98% of the hydraulic head, indicating that it provides an effective seepage control performance. In the vicinity of the No. 1 drainage tunnel on the right bank and the underground powerhouse on the left bank, as well as the surrounding area, dis-

tinct drawdown funnels are observed, suggesting that the drainage system can effectively reduce the hydraulic head and pore water pressure, thereby ensuring the operational safety of the underground powerhouse.

At the same location, a higher upstream water level generally results in a larger seepage gradient. For example, the hydraulic gradients calculated under the normal pool level of 275.00 m are greater than those under the flood-limited water level of 248.00 m. Under high-water-level conditions, relatively large seepage gradients occur within a certain range near the top of the core wall, generally ranging from 2.5 to 2.8 at the water level of 275.00 m. During the dam design stage, systematic seepage tests were conducted on various dam materials. The permeability coefficient of the silty loam used in the core wall was determined to be in the range of 1×10^{-8} to 1×10^{-7} cm/s. When the soil remains intact, its critical hydraulic gradient can exceed 200; after cracking occurs, the critical hydraulic gradient decreases to approximately 20~30. In all calculated operating conditions, the seepage gradients within the core wall remain below 3.0, satisfying the design requirements. The hydraulic gradients in the remaining zones generally range from 1.0 to 2.0. Therefore, the reservoir can operate safely under the water level of 275.00 m.

When dissolution-induced aging occurs in the foundation cut-off wall, the hydraulic gradients on both the upstream and downstream sides of the foundation cut-off wall decrease to some extent, whereas the hydraulic gradients at the cofferdam cut-off wall, downstream seepage exit, top of the core wall, and seepage exit of the core wall remain essentially unchanged. When dissolution-induced aging occurs in the core wall, the hydraulic gradients at the top of the core wall, seepage exit of the core wall, and cofferdam cut-off wall decrease slightly, while the hydraulic gradient at the foundation cut-off wall increases significantly. With an increase in the thickness of the sediment layer, the hydraulic gradients at the cofferdam cut-off wall and foundation cut-off wall decrease, whereas those at the top of the core wall, the seepage exit of the core wall, and the downstream seepage exit remain nearly unchanged, indicating a limited influence. Therefore, an increase in the thickness of the sediment layer provides an auxiliary seepage control effect for the vertical seepage control system.

6.2 Seepage Control and Drainage Performance Analysis

The horizontal seepage control system exhibits a certain seepage control effect. In particular, with the increase in the thickness of the upstream sediment layer, it can reduce the hydraulic gradient of the vertical seepage control system and effectively dissipate the hydraulic head, thereby providing a favorable auxiliary seepage control effect for the cofferdam cut-off wall and the foundation cut-off wall. Based on the hydraulic head distribution diagrams, hydraulic gradients, and calculated seepage discharge results for different sections, the grout curtains in the dam foundation and the rock masses on both banks do not exhibit a particularly pronounced seepage control effect. The dissipation of hydraulic head is mainly achieved by the sediment layer, cofferdam cut-off wall, foundation cut-off wall, and core wall, with the overall hydraulic head dissipation exceeding 98%. The horizontal and vertical seepage control systems jointly constitute an integrated seepage control system. When the thickness of the upstream sediment layer

increases, the influence of the horizontal seepage control system becomes more significant. When dissolution-induced aging occurs in the core wall, the foundation cut-off wall can effectively compensate for the function of the vertical seepage control system. Overall, the seepage control system of this hydraulic project performs well and can effectively reduce the hydraulic gradient, dissipate the hydraulic head, and decrease seepage discharge.

Drainage curtains are installed in the rock masses on both the left and right banks of the project, and drawdown funnels of groundwater level are observed near the drainage curtains on both banks. On the right bank, the groundwater level downstream of the dam is lower than 200 m, and the groundwater level at the center of the drawdown funnel is lower than 130 m. On the left bank, the groundwater level downstream of the dam is also lower than 200 m, and the center of the drawdown funnel is located in the powerhouse area, where the groundwater level is lower than 100 m. This can ensure the groundwater-level safety of the powerhouse.

Table 7 presents the calculated seepage discharges from the drainage tunnels on the left and right banks under various operating conditions. Under normal reservoir operation, the seepage discharges on the left and right banks are 6324.4 m^3/d and 2333.8 m^3/d, respectively. When dissolution-induced aging occurs in the foundation seepage control system, the seepage discharge on the left bank increases significantly, whereas that on the right bank shows no obvious change. When dissolution-induced aging occurs in the powerhouse seepage control system, the seepage discharge on the left bank also increases significantly. Variations in the thickness of the sediment layer have little influence on the seepage discharges on both banks, but they can reduce seepage discharge through the dam foundation.

Table 7. Summary table for calculation of leakage on left and right banks and dam foundation

	Water level	Working conditions	Seepage of each drainage tunnel on the left bank					Total left bank	Leakage of right bank drainage tunnel (m^3/d)	Leakage of dam foundation (m^3/d)	Total (m^3/d)
			Caves 2 and 3	Cave 4	Caves 28 and 30	workshop side wall	Top arch				
normal operation	275	normal operation	147.4	244.2	5828.2	104.6		6324.4	2333.8	7625.2	16283.4
Anti-seepage corrosion aging of dam foundation	275	$5K_0$	155.1	280.9	6574.5	104.9		7115.4	3031.2	7743.1	17889.7
		$10K_0$	157.5	287.8	6731.3	104.9		7281.6	2720.7	8015.2	18017.5
		$100K_0$	166.1	304.5	7070.5	105.4		7646.4	3018.2	8626.7	19291.3
Anti-seepage corrosion aging of workshop	275	$5K_0$	147.4	283.6	6468.4	104.8		7004.2	2333.8	7689.4	17027.4
		$10K_0$	147.4	287.6	6322.8	104.6		6862.4	2333.8	7735.5	16931.7
		$20K_0$	147.4	292.2	6450.4	104.6		6994.7	2333.8	7805.2	17133.7
Thickness change of silting layer	275	plus 5m	147.4	244.2	5828.2	104.6		6324.4	2333.8	7508.3	16166.5
		plus 10m	147.4	244.2	5828.2	104.6		6324.4	2333.8	7108.3	15766.5
		plus 20m	147.4	244.2	5828.2	104.6		6324.4	2333.8	6768.8	15427.0

7 Conclusion

(1) In this paper, a three-dimensional numerical groundwater flow model of the study area is established, incorporating strata lithology, the underground powerhouse, dam body, dam foundation, mountain bodies on both banks, faults, drainage tunnels, anti-seepage facilities, and sedimentary layers. The model parameters are identified and validated via the structural plane control method. The calculated groundwater levels and seepage rates are in good agreement with the measured results, satisfying the accuracy requirements.

(2) The distribution of seepage field shows obvious regularity under various working conditions. The seepage control effect of the core wall is obvious, which controls and reduces the position of the dam saturation line. The seepage control effect of the upstream silting layer, cofferdam and dam foundation cutoff wall is also very obvious. The whole seepage control system can reduce the hydraulic head by more than 98%. When the thickness of the silting layer increases, the seepage control effect becomes more and more obvious, and the escape point of the downstream surface of the core wall is basically consistent with the downstream water level.

(3) The hydraulic gradient is generally small, and the possibility of seepage failure is very small. At the top of the core wall and the cutoff wall of the dam foundation, the hydraulic gradient is relatively high, basically maintained at 2.5~3.5, and the hydraulic gradient in other parts is generally between 1.0~2.0, and the hydraulic gradient at the exit is very small, and the hydraulic gradient at the core wall and dam foundation is less than the critical hydraulic gradient, so it can operate safely under the condition of 275m water level.

(4) It can be seen from the contour map of groundwater level under various working conditions that there are obvious water level drop funnels at the drainage tunnel, with the water level behind the left and right bank dams lower than 200m, the water level in the center of the right bank drop funnel lower than 130m, and the water level in the center of the left bank drop funnel lower than 100m, indicating that the drainage system of this project has good operation effect. By simulating the leakage of the hub under various working conditions, it is concluded that the seepage control effect of dam foundation and factory building area is good, which can effectively reduce the leakage.

(5) On the whole, the anti-seepage system of the water control project has a good effect, which can effectively reduce the hydraulic gradient, reduce the head and reduce the leakage.

Acknowledgments

This study was supported by Major Science and Technology Projects of the Ministry of Water Resources (SKS-2025027); National Natural Science Foundation of China(U23B20150); Central Public-interest Scientific Institution Basal Research Fund (Yj726011).

References

1. Wang, N.X., Zhang, W.M., Gu, X.W., et al. Centrifugal model test study on seepage characteristics of core wall of high rockfill dam. Rock and Soil Mechanics, 34(10), 2769-2773+2780 (2013). DOI: 10.16285/j.rsm.2013.10.024.
2. Janabi A S M A ,Dibs H ,Sammen S S , et al.Comparison Analysis of Seepage Through Homogenous Embankment Dams Using Physical, Mathematical and Numerical Models[J].Arabian Journal for Science and Engineering,2024,50(11):1-10. DOI:10.1007/S13369-024-09224-X.
3. Dai, Q.W., Zhu, Z.L., Han, X.J., et al. Forward modeling of saturated-unsaturated seepage in earth-rock dams based on element-free Galerkin method. Journal of Water Resources and Water Engineering, 34(2), 171-179 (2023).
4. Zhao, S.F., Xu, L.Q., Zhang, H.W., et al. Reliability analysis of service life of extra-high earth-core rockfill dam considering seepage and dissolution effect of dam foundation anti-seepage body. Journal of Hydraulic Engineering, 55(11), 1391-1403+1416 (2024). DOI: 10.13243/j.cnki.slxb.20230726.
5. ZHANG Wenbing, LI Qingming, LI Mingchao, et al. Study on the long-term service performance of anti-seepage walls of earth-rock dams under coupled effect of seepage and calcium leaching[J]. Journal of Hydraulic Engineering, 2025, 56(10): 1314-1325.
6. Yaseen, Z.M., Al-Hetari, M. & Ali, U. Earth and Rockfill Dams' Seepage Prediction Using Artificial Intelligence Models: A Comprehensive Review Assessment, and Future Research Directions. Arch Computat Methods Eng 33, 4755–4791 (2026).DOI: 10.1007/s11831-025-10433-2
7. Zhou C ,Shen Z ,Xu L , et al.Durability analysis method for plastic concrete cutoff walls considering the coupling effects of dissolution-seepage-stress[J].Construction and Building Materials,2025,477141318-141318.DOI:10.1016/J.CONBUILDMAT.2025.141318.
8. Zhang W ,Chen Y ,Yuan Y , et al.Numerical insights into the calcium leaching characteristics and service durability of roller-compacted concrete dams[J].Structures,2025,80109945-109945.DOI:10.1016/J.ISTRUC.2025.109945.
9. Huo J ,Ma F ,Ji X .Porosity and permeability variations of a dam curtain during dissolution[J].Water Science and Engineering,2019,12(2):155-161.
10. Wang, R.X., Wang, R.J., Zhao, Y. Sensitivity analysis of seepage field of high earth-rock cofferdam on deep overburden. Journal of Water Resources and Water Engineering, 28(6), 215-218+225 (2017).

Open Access This chapter is licensed under the terms of the Creative Commons Attribution-NonCommercial 4.0 International License (http://creativecommons.org/licenses/by-nc/4.0/), which permits any noncommercial use, sharing, adaptation, distribution and reproduction in any medium or format, as long as you give appropriate credit to the original author(s) and the source, provide a link to the Creative Commons license and indicate if changes were made.

The images or other third party material in this chapter are included in the chapter's Creative Commons license, unless indicated otherwise in a credit line to the material. If material is not included in the chapter's Creative Commons license and your intended use is not permitted by statutory regulation or exceeds the permitted use, you will need to obtain permission directly from the copyright holder.

